Magnetospheric chaos and dynamical complexity response during storm time disturbance

Irewola Aaron Oludehinwa[1], Olasunkanmi Isaac Olusola[1], Olawale Segun Bolaji[1,2], Olumide Olayinka Odeyemi[1], Abdullahi Ndzi Njah[1]

[1]Department of Physics, University of Lagos, Nigeria

[2]Department of Physics, University of Tasmania, Australia

Abstract

In this study, we examine the magnetospheric chaos and dynamical complexity response to the disturbance storm time (D_{st}) and solar wind electric field (VB_s) during different categories of geomagnetic storm (minor, moderate and major geomagnetic storm). The time series data of the D_{st} and VB_s are analyzed for the period of nine years using nonlinear dynamics tools (Maximal Lyapunov Exponent, MLE, Approximate Entropy, ApEn and Delay Vector Variance, DVV). We found a significant trend between each nonlinear parameter and the categories of geomagnetic storm. The MLE and ApEn values of the D_{st} indicate that chaotic and dynamical complexity responses are high during minor geomagnetic storms, reduce at moderate geomagnetic storms and decline further during major geomagnetic storms. However, the MLE and ApEn values obtained from VB_s indicate that chaotic and dynamical complexity responses are high with no significant difference between the periods that are associated with minor, moderate and major geomagnetic storms. The test for nonlinearity in the D_{st} time series during major geomagnetic storm reveals the strongest nonlinearity features. Based on these findings, the dynamical features obtained in the VB_s as input and D_{st} as output of the magnetospheric system suggest that the magnetospheric dynamics is nonlinear and the solar wind dynamics is consistently stochastic in nature.

Keywords: D_{st} signals, Solar wind electric field (VB_s) signals, Geomagnetic storm, Chaotic behaviour, Dynamical complexity, Nonlinearity.

1.0 Introduction

The response of chaos and dynamical complexity behaviour with respect to magnetospheric dynamics varies (Tsurutani et al., 1990). This is due to changes in the interplanetary electric fields imposed on the magnetopause and those penetrating the inner magnetosphere and sustaining convection thereby initiating geomagnetic storm (Dungey, 1961; Pavlos et al., 1992). A prolonged southward turning of interplanetary magnetic field (IMF,B_z), which indicates that solar wind-magnetosphere coupling is in-progress was confirmed on many occasions for which such geomagnetic storm was driven by Corotating Interaction Regions (CIRs), or by the sheath preceding an interplanetary coronal mass ejection (ICME) or by a combination of the sheath and an ICME magnetic cloud (Gonzalez and Tsurutani, 1987; Tsurutani and Gonzalez, 1987; Tsurutani et al., 1988; Cowley, 1995; Tsutomu, 2002; Yurchyshyn et al., 2004; Kozyra et al., 2006; Echer et al., 2008; Meng et al., 2019; Tsurutani et al., 2020). The sporadic magnetic reconnection between the southward component of the Alfven waves and the earth's magnetopause leads to isolated substorms/convection events such as the high intensity long-duration continuous AE activity (HILDCAA) which are shown to last from days to weeks (Akasofu, 1964; Tsurutani et al., 1972; Meng et al., 1973; Tsurutani and Gonzalez, 1987; Hajra et al., 2013; Liou et al., 2013; Mendes et al., 2017; Hajra and Tsurutani, 2018; Tsurutani and Hajra, 2021). Notably, the introduction of Disturbance Storm Time (D_{st}) index (Sugiura, 1964; Sugiura and Kamei, 1991) unveiled the quantitative measure of the total energy of the ring current particles. Therefore, the D_{st} index remains one of the most popular global indicators that can precisely reveal the severity of a geomagnetic storm (Dessler and Parker, 1959).

The D_{st} fluctuations exhibit different signatures for different categories of geomagnetic storm. Ordinarily, one can easily anticipate that fluctuations in a D_{st} signal appear chaotic and complex.

These may arise from the changes in the interplanetary electric fields driven by the solar wind-magnetospheric coupling processes. At different categories of geomagnetic storm, fluctuations in the D_{st} signals differ (Oludehinwa et al., 2018). One obvious reason is that as the intensity of the geomagnetic storm increases, the fluctuation behaviour in the D_{st} signal becomes more complex and nonlinear in nature. It has been established that the electrodynamic response of the magnetosphere to solar wind drivers are non-autonomous in nature (Price and Prichard, 1993; Price et al., 1994; Johnson and Wings, 2005). Therefore, the chaotic analysis of the magnetospheric time series must be related to the concept of input-output dynamical process (Russell et al., 1974; Burton et al.,1975; Gonzalez et al., 1989; Gonzalez et al., 1994). Consequently, it is necessary to examine the chaotic behaviour of the solar wind electric field (VB_s) as input signals and the magnetospheric activity index (D_{st}) as output during different categories of geomagnetic storms.

Several works have been presented on the chaotic and dynamical complexity behaviour of the magnetospheric dynamics based on autonomous concept, i.e using the time series data of magnetospheric activity alone such as auroral electrojet (AE), Amplitude Lower (AL) and D_{st} index (Vassiliadis et al.,1990; Baker and Klimas, 1990; Vassiliadis et al.,1991; Shan et al., 1991; Pavlos et al., 1994; Klimas et al., 1996; Valdivia et al., 2005; Mendes et al., 2017; Consolini, 2018). They found evidence of low-dimensional chaos in the magnetospheric dynamics. For instance, the report by Vassiliadis et al. (1991) shows that the computation of Lyapunov exponent for AL index time series gives a positive value of Lyapunov exponent indicating the presence of chaos in the magnetospheric dynamics. Unnikrishnan, (2008) studied the deterministic chaotic behaviour in the magnetospheric dynamics under various physical conditions using AE index time series and found that the seasonal mean value of Lyapunov exponent in winter season during quiet

periods ($0.7 \pm 0.11\, min^{-1}$) is higher than that of the stormy periods ($0.36 \pm 0.09\, min^{-1}$). Balasis et al. (2006) examined the magnetospheric dynamics in the D_{st} index time series from pre-magnetic storm to magnetic storm period using fractal dynamics. They found that the transition from anti-persistent to persistent behaviour indicates that the occurrence of an intense geomagnetic storm is imminent. Balasis et al. (2009) further reveal the dynamical complexity behaviour in the magnetospheric dynamics using various entropy measures. They reported a significant decrease in dynamical complexity and an accession of persistency in the D_{st} time series as the magnetic storm approaches. Recently, Oludehinwa et al. (2018) examined the nonlinearity effects in D_{st} signals during minor, moderate and major geomagnetic storm using recurrence plots and recurrence quantification analyses. They found that the dynamics of the D_{st} signal is stochastic during minor geomagnetic storm periods and deterministic as the geomagnetic storm increases.

Also, studies describing the solar wind and magnetosphere as a non-autonomous system have been extensively investigated. Price et al. (1994) examine the nonlinear input-output analysis of AL index and different combinations of interplanetary magnetic field (IMF) with solar wind parameters as input functions. They found that only a few of the input combinations show any evidence whatsoever for nonlinear coupling between the input and output for the interval investigated. Pavlos et al. (1999) presented further evidence of magnetospheric chaos. They compared the observational behaviour of the magnetospheric system with the results obtained by analyzing different types of stochastic and deterministic input-output systems and asserted that a low dimensional chaos is evident in magnetospheric dynamics. Devi et al. (2013) studied the magnetospheric dynamics using AL index and the southward component of IMF(B_z). They observed that the magnetosphere and turbulent solar wind have values corresponding to nonlinear dynamical system with chaotic behaviour. The modeling and forecasting approach have been

applied to magnetospheric time series using nonlinear models (Valdivia et al., 1996; Vassiliadis et al., 1999; Vassiliadis, 2006; Balikhin et al., 2010). These efforts have improved our understanding that the concept of nonlinear dynamics can reveal some hidden dynamical information in the observational time series. In addition to these nonlinear effects in D_{st} signals, a measure of the exponential divergence and convergence within the trajectories of a phase space known as Maximal Lyapunov Exponent (MLE), which has the potential to depict the chaotic behavior in the D_{st} and VB_s time series during a minor, moderate and major geomagnetic storm have not been investigated. In addition, to the best of our knowledge, computation of Approximate Entropy (ApEn) that depicts the dynamical complexity behaviour during different categories of geomagnetic storm has not been reported in the literature. The test for nonlinearity through delay vector variance (DVV) analysis that reveals the nonlinearity features in D_{st} and VB_s time series during minor, moderate and major geomagnetic storms is not well known. It is worth to note that understanding the dynamical characteristics in the D_{st} and VB_s signals at different categories of geomagnetic storms will provide useful diagnostic information to different conditions of space weather phenomenon. Consequently, this study attempts to carry out comprehensive numerical analyses to unfold the chaotic and dynamical complexity behaviour in the D_{st} and VB_s signals during minor, moderate and major geomagnetic storm. In section 2, our methods of data acquisition are described. Also, the nonlinear analysis that we employed in this investigation are detailed. In section 3, we unveiled our results and engage the discussion of results in section 4.

2.0 Description of the Data and Nonlinear Dynamics

The D_{st} index is derived by measurements from ground-based magnetic stations at low-latitudes observatories around the world and depicts mainly the variation of the ring current, as well as the Chapman-Ferraro Magnetopause currents, and tail currents to a lesser extent (Sugiura, 1964;

Feldstein et al., 2005; Feldstein et al., 2006; Love and Gannon, 2009). Due to its global nature, D_{st} time series provides a measure of how intense a geomagnetic storm was (Dessel and Parker, 1959). In this study, we considered D_{st} data for the period of nine years from January to December between 2008 and 2016 which were downloaded from the World Data Centre for Geomagnetism, Kyoto, Japan (http://wdc.kugi-kyoto-u.ac.jp/Dstae/index.html). We use the classification of geomagnetic storms as proposed by Gonzalez et al. (1994) such that D_{st} index value in the ranges $0 \leq Dst \leq -50nT$, $-50nT \leq Dst \leq -100nT$, $-100nT \leq Dst \leq -250nT$ are classified as minor, moderate and major geomagnetic storms respectively and each time series is being classified based on its minimum D_{st} value. The solar wind electric field (VB_s) data are archived from the National Aeronautics and Space Administration, Space Physics Facility (http://omniweb.gsfc.nasa.gov). The sampling time of D_{st} and VB_s time series data was 1-hour. It is well known that the dynamics of the solar wind contribute to the driving of the magnetosphere (Burton et al. 1975). Furthermore, we took the solar wind electric field (VB_s) as the input signal (Price and Prichard, 1993; Price et al., 1994). The VB_s was categorized according to the periods of minor, moderate and major geomagnetic storm. Then, the D_{st} and VB_s time series were subjected to a variety of nonlinear analytical tools explained as follow:

2.1 Phase Space Reconstruction and Observational time series

An observational time series can be defined as a sequence of scalar measurements of some quantity, which is a function of the current state of the system taken at multiples of a fixed sampling time. In nonlinear dynamics, the first step in analyzing an observational time series data is to reconstruct an appropriate state space of the system. Takens (1981) and Mane (1981) stated that one time series or a few simultaneous time series are converted to a sequence of vectors. This

reconstructed phase space has all the dynamical characteristic of the real phase space provided the time delay and embedding dimension are properly specified.

$$X(t) = [x(t), x(t+\tau), x(t+2\tau), \dots, x(t+(m-1)\tau]^T \quad (1)$$

Where $X(t)$ is the reconstructed phase space, $x(t)$ is the original time series data, τ is the time delay and m is the embedding dimension. An appropriate choice of τ and m are needed for the reconstruction of phase space which is determined by average mutual information and false nearest neighbor, respectively.

2.2 Average Mutual Information (AMI)

The method of Average Mutual Information (AMI) is one of the nonlinear techniques used to determine the optimal time delay (τ) required for phase space reconstruction in observational time series. The time delay mutual information was proposed by Fraser and Swinney, (1986) instead of an autocorrelation function. This method takes into account nonlinear correlations within the time series data. It measures how much information can be predicted about one time series point, given full information about the other. For instance, the mutual information between x_i and $x_{(i+\tau)}$ quantifies the information in state $x_{(i+\tau)}$ under the assumption that information at the state x_i is known. The AMI for a time series, $x(t_i), \quad i = 1,2, \dots, N$ is calculated as:

$$I(T) = \sum_{x(t_i),\ x(t_i+T)} P(x(t_i), x(t_i+T)) \times \log_2 \left[\frac{P(x(t_i), x(t_i+T))}{P(x(t_i))\, P(x(t_i+T))}\right] \quad (2)$$

where $x(t_i)$ is the ith element of the time series, $T = k\Delta t \quad (k = 1,2, \dots, k_{max})$, $P(x(t_i))$ is the probability density at $x(t_i)$, $P(x(t_i), x(t_i+T))$ is the joint probability density at the pair $x(t_i), x(t_i+T)$. The time delay (τ) of the first minimum of AMI is chosen as optimal time delay (Fraser and Swinney, 1986). Therefore, the AMI was applied to the D_{st} and VB_s time series and

the plot of AMI versus time delay is shown in Figure (3). We notice that the AMI showed the first local minimum at roughly $\tau = 15hr$. Furthermore, the values of τ near this value of ~15hr maintain constancy for both VB_s and D_{st}. In the analysis $\tau = 15hr$ was used as the optimal time delay for the computation of maximal Lyapunov exponent.

2.3 False Nearest Neighbor (FNN)

In determining the optimal choice of embedding dimension(m), the false nearest neighbor method was used in the study. The method was suggested by Kennel et al. (1992). The concept is based on how the number of neighbors of a point along a signal trajectory changes with increasing embedding dimension. With increasing embedding dimension, the false neighbor will no longer be neighbors, therefore by examining how the number of neighbors changes as a function of dimension, an appropriate embedding dimension can be determined. For instance, suppose we have a one-dimensional time series. We can construct a time series $y(t)$ of D-dimensional points from the original one-dimensional time series $x(t)$ as follows:

$$y(t) = (x(t), x(t+\tau), \dots, x(t+(D-1)\tau) \quad (3)$$

where τ and D are time delay and embedding dimension. Using the formular from Kennel et al. (1992); Wallot and Monster, (2018), if we have a D-dimensional phase space and denote the rth nearest neighbor of a coordinate vector $y(t)$ by $y^{(r)}(t)$, then the square of the Euclidean distance between $y(t)$ and the rth nearest neighbor is:

$$R_D^2(t,r) = \sum_{k=0}^{D-1} \left[x(t+k\tau) - x^{(r)}(t+k\tau)\right]^2 \quad (4)$$

Now applying the logic outlined above, we can go from a D-dimensional phase space to $(D+1)$ dimensional phase space by time-delay embedding, adding a new coordinate to $y(t)$, and ask what is the squared distance between $y(t)$ and the same rth nearest neighbor:

$$R_{D+1}^2(t,r) = R_D^2(t,r) + \left[x(t+D\tau) - x^{(r)}(t+D\tau)\right]^2 \qquad (5)$$

As explained above, if the one-dimensional time series is already properly embedded in D dimensions, then the distance R between $y(t)$ and the rth nearest neighbor should not change appreciably by some distance criterion $R_{tol}(i.e\ R < R_{tol})$. Moreover, the distance of the nearest neighbor when embedded into the next higher dimension relative to the size of the attractor should be less than some criterion $A_{tol}(i.e\ R_{D+1} < A_{tol})$. Doing this for the nearest neighbor of each coordinate will result on many false nearest neighbors when embedding is insufficient or in few (or no) false neighbors when embedding is sufficient. In the analysis, the FNN was applied to the D_{st} and VB_s time series to detect the optimal value of embedding dimension(m). Figure (4) shows a sample plot of the percentage of false nearest neighbor against embedding dimension in one of the months under investigation (other months show similar results, thus for brevity we depict only one of the results). We notice that the false nearest neighbor attains its minimum value at $m \geq 5$ indicating that embedding dimension (m) from $m \geq 5$ are optimal values. Therefore, $m = 5$ was used for the computation of maximal Lyapunov exponent.

2.4 Maximal Lyapunov Exponent (MLE)

The Maximal Lyapunov Exponent (MLE) is one of the most popular nonlinear dynamics tool used for detecting chaotic behaviour in a time series data. It describes how small changes in the state of a system grow at an exponential rate and eventually dominate the behaviour. An important indication of chaotic behavior of a dissipative deterministic system is the existence of a positive

Lyapunov Exponent. A positive MLE signifies divergence of trajectories in one direction or expansion of an initial volume in this direction. On the other hand, a negative MLE exponent implies convergence of trajectories or contraction of volume along another direction. The algorithm proposed by Wolf et al. (1985) for estimating MLE is employed to compute the chaotic behavior of the D_{st} and VB_s time series at minor, moderate and major geomagnetic storm. Other methods of determining MLE includes Rosenstein's method, Kantz's method and so on. In this study, the MLE at minor, moderate and major geomagnetic storms periods was computed with $m = 5$ and $\tau = 15hr$ as shown in figures (5 & 6-bar plots) for D_{st} and VB_s. The calculation of MLE is explained as follows: given a sequence of vector $x(t)$, an m-dimensional phase space is formed from the observational time series through embedding theorem as

$$\{x(t), x(t+\tau), \dots, x(t+(m-1)\tau)\} \quad (6)$$

where m and τ are as defined earlier, after reconstructing the observational time series, the algorithm locates the nearest neighbor (in Euclidean sense) to the initial point $\{x(t_0), \dots, x(t_0 + (m-1)\tau\}$ and denote the distance between these two points $L(t_0)$. At a later point t_1, the initial length will have evolved to length $L'(t_1)$. Then the MLE is calculated as:

$$\lambda = \frac{1}{t_M - t_0} \sum_{k=1}^{M} \log_2 \frac{L'(t_k)}{L(t_{k-1})} \quad (7)$$

M is the total number of replacement steps. We look for a new data point that satisfies two criteria reasonably well: its separation, $L(t_1)$, from the evolved fiducial point is small. If an adequate replacement point cannot be found, we retain the points that were being used. This procedure is repeated until the fiducial trajectory has traversed the entire data.

2.5 Approximate Entropy (ApEn)

Approximate Entropy (ApEn) is one of the nonlinear dynamics tools that measure the dynamical complexity in observational time series. The concept was proposed by Pincus, (1991) which provides a generalized measure of regularity, such that it accounts for the logarithm likehood in the observational time series. For instance, a dataset of length, N, that repeat itself for m points within a boundary will again repeat itself for $m+1$ points. Because of its computational advantage, ApEn has been widely used in many areas of disciplines to study dynamical complexity (Pincus and Kalman (2004); Pincus and Goldberger (1994); McKinley et al. (2011); Kannathan et al. (2005); Balasis et al. (2009); Shujuan and Weidong, (2010); Moore and Marchant (2017)). The ApEn is computed using the formula below:

$$ApEn(m,r,N) = \frac{1}{N-m+1}\sum_{i=1}^{N-m+1}\log C_i^m(r) - \frac{1}{N-m}\sum_{i=1}^{N-m}\log C_i^m(r) \quad (8)$$

where $C_i^m(r) = \frac{1}{N-m+1}\sum_{j=1}^{N-m+1}\Theta\left(r - \left\|x_i - x_j\right\|\right)$ is the correlation integral, m is the embedding dimension and r is the tolerance. To compute the ApEn for the D_{st} and VB_s time series classified as minor, moderate and major geomagnetic storm from 2008 to 2016, we choose $(m=3, \tau = 1hr)$. We refer the works of Pincus, (1991); Kannathal et al. (2005); and Balasis et al. (2009) to interested readers where all the computational steps regarding ApEn were explained in details. Figures (5 & 6) depict the stem plot of ApEn for D_{st} and (VB_s) from 2008 to 2016.

2.6 Delay Vector Variance (DVV) analysis

The Delay Vector Variance (DVV) is a unified approach in analyzing and testing for nonlinearity in a time series (Gautama et al., 2004; Mandic et al., 2007). The basic idea of the DVV is that, if two delay vectors of a predictable signal are close to each other in terms of the Euclidean distance,

they should have similar target. For instance, when a time delay (τ) is embedded into a time series $x(k),\ k = 1,2,\dots,N$, then a reconstructed phase space vector is formed which represents a set of delay vectors (DVs) of a given dimension.

$$X(k) = [X_{k-m\tau}, \dots, X_{k-\tau}]^T \tag{9}$$

Reconstructing the phase space, a set (λ_k) is generated by grouping those DVs that are with a certain Euclidean distance to DVs $\big(X(k)\big)$. For a given embedding dimension (m), a measure of unpredictability $\sigma *^2$ is computed over all pairwise Euclidean distance between delay vector as

$$d(i,j) = \|x(i) - x(j)\| \quad (i \neq j) \tag{10}$$

Then, sets $\lambda_k(r_d)$ are generated as the sets which consist of all delay vectors that lie closer to $x(k)$ than a certain distance r_d.

$$\lambda_k(r_d) = \{x(i) \| x(k) - x(i)\| \leq r_d\} \tag{11}$$

For every set $\lambda_k(r_d)$, the variance of the corresponding target $\sigma *^2\ (r_d)$ is

$$\sigma *^2\ (r_d) = \frac{\frac{1}{N}\sum_{k=1}^{N} \sigma_k^2(r_d)}{\sigma_k} \tag{12}$$

where $\sigma *^2\ (r_d)$ is target variance against the standardized distance indicating that Euclidean distance will be varied in a manner standardized with respect to the distribution of pairwise distance between DVs. Iterative Amplitude Adjusted Fourier Transform (IAAFT) method is used to generate the surrogate time series (Kugiumtzis, 1999). If the surrogate time series yields DV plots similar to the original time series and the scattered plot coincides with the bisector line, then the original time series can be regarded as linear (Theiler et al., 1992; Gautama et al., 2004; Imitaz, 2010; Jaksic et al., 2016). On the other hand, if the surrogate time series yields DV plot that is not

similar to that of the original time series, then the deviation from the bisector lines indicates nonlinearity. The deviation from the bisector lines grows as a result of the degree of nonlinearity in the observational time series.

$$t^{DVV} = \sqrt{\langle(\sigma^{*2}(r_d) - \frac{\sum_{i=1}^{N} \sigma_{s,i}^{*2}}{N_s})\rangle} \quad (13)$$

where $\sigma_{s,i}^{*2}(r_d)$ is the target variance at the span r_d for the i^{th} surrogate. To carry out the test for nonlinearity in the D_{st} signals, $m = 3$ and $n_d = 3$, the number of reference DVs=200, and number of surrogate, $N_s = 25$ was used in all the analysis. Then we examined the nonlinearity response at minor, moderate and major geomagnetic storm.

3.0 Results

In this study, D_{st} and VB_s time series from January to December were analyzed for the period of nine years (2008 to 2016) to examine the chaotic and dynamical complexity response in the magnetospheric dynamics during minor, moderate and major geomagnetic storms. Figures (1) & (2), display the samples of fluctuation signatures of D_{st} and VB_s signals classified as (a): minor, (b): moderate and (c): major geomagnetic storms. The plot of Average Mutual information against time delay (τ) shown in Figure (3) depicts that the first local minimum of the AMI function was found to be roughly at $\tau = 15$hr. Furthermore, we notice that the values of τ near this value of (~15hr) maintain constancy for both VB_s and D_{st}. Also, in Figure (4), we display the plot of the percentage of false nearest neighbor against embedding dimension (m). It is obvious that a decrease in false nearest neighbor when increasing the embedding dimension drop steeply to zero at the optimal dimension($m = 5$), thereafter the false neighbors stabilizes at that $m = 5$ for VB_s and D_{st}. Therefore, $m = 5$ and $\tau = 15$hr was used for the computation of MLE at different categories of geomagnetic storm, while $m = 3$ and $\tau = 1$hr are applied for the computation of ApEn values.

The results of MLE (bar plot) and ApEn (stem plot) for D_{st} at minor, moderate and major geomagnetic storms are shown in Figure 5. During minor geomagnetic storms, we notice that the value of MLE ranges between 0.07 and 0.14 for most of the months classified as minor geomagnetic storm. Similarly, the ApEn (stem plot) ranges between 0.59 and 0.83. It is obvious that strong chaotic behaviour with high dynamical complexity are associated with minor geomagnetic storms. During moderate geomagnetic storms, (see b part of Figure 5), we observe a reduction in MLE values $(0.04 - 0.07)$ compared to minor geomagnetic storm periods. Within the observed values of MLE during moderate geomagnetic storms, we found a slight rise of MLE

in the following months (Mar 2008), (Apr 2011), (Jan 2012, Feb 2012, Apr 2012), (Jul 2015, Aug 2015, Sept 2015, Oct 2015, Nov 2015) and (Nov 2016). Also, the ApEn revealed a reduction in values between 0.44 and 0.57 during moderate geomagnetic storms. The lowest values of ApEn were noticed in the following months: May 2010, Mar 2011, and Jan 2016. During major geomagnetic storms as shown in Figure 5, the minimum and maximum value of MLE is respectively 0.03 and 0.04 implying a very strong reduction of chaotic behaviour compared with minor and moderate geomagnetic storms. The lowest values of MLE were found in the months of Jul 2012, Jun 2013 and Mar 2015. Interestingly, further reduction in ApEn value $(0.29 - 0.40)$ was as well noticed during this period. Thus, during major geomagnetic storms, chaotic behaviour and dynamical complexity subside significantly.

We display in Figure 6, the results of MLE and ApEn computation for the VB_s which has been categorized according to the periods of minor, moderate and major geomagnetic storms. The values of MLE (bar plot) were between 0.06 and 0.20 for VB_s. The result obtained indicate strong chaotic behaviour with no significant difference in chaoticity during minor, moderate and major geomagnetic storm. Similarly, the results obtained from computation of ApEn (stem plot) for VB_s depict a minimum value of 0.60 and peak value of 0.87 as shown in Figure 6. The ApEn values of VB_s indicates high dynamical complexity response with no significant difference during the periods of the three categories of geomagnetic storm investigated.

The test for nonlinearity in the D_{st} signals during minor, moderate and major geomagnetic storms was analyzed through the DVV analysis. Shown in Figure 9 is the DVV plot and DVV scatter plot during minor geomagnetic storm for January 2009 and January 2014. We found that the DVV plots during minor geomagnetic storms reveals a slight separation between the original and surrogate data. Also, the DVV scatter plots shows a slight deviation from the bisector line between

317 the original and surrogate data which implies nonlinearity. Also, during moderate geomagnetic
318 storms, we notice that the DVV plot depicts a wide separation between the original and the
319 surrogate data. Also, a large deviation from the bisector line between the original and the surrogate
320 data was also noticed in the DVV scatter plot as shown in Figure (8) thus indicating nonlinearity.
321 In Figure (9), we display samples of DVV plot and DVV scatter plot during major geomagnetic
322 storm for Oct 2011 and Dec 2015. The original and the surrogate data showed a very large
323 separation in the DVV plot during major geomagnetic storm. While the DVV scatter plot depict
324 the greatest deviation from the bisector line between the original and the surrogate data which is
325 also an indication of nonlinearity. The DVV analysis of the VB_s time series during minor, moderate
326 and major geomagnetic storms shown in Figures (10-12) revealed a separation between the original
327 and surrogate data with no significant difference between the periods of minor, moderate and major
328 geomagnetic storm.

329 **4.0 Discussion of Results**

330 **4.1 The chaotic and dynamical complexity response in D_{st} at minor, moderate and major**
331 **geomagnetic storms**

332 Our result shows that the values of MLE for D_{st} during minor geomagnetic storm are higher,
333 indicating significant chaotic response during minor geomagnetic stormy periods (bar plot, Figure
334 5). This increase in chaotic behaviour for D_{st} signals during minor geomagnetic storms may be as
335 a result of asymmetry features in the longitudinal distribution of solar source region for the
336 Corotating Interaction Regions (CIR) signatures responsible for the development of geomagnetic
337 storms (Turner et al. 2006; Kozyra et al. 2006). CIR generated magnetic storms are generally
338 weaker than ICME/MC generated storms (Gonzalez et al., 1994; Tsurutani et al., 1995; Feldstein
339 et al., 2006; Richardson and Cane, 2011). Therefore, we suspect that the increase in chaotic

behaviour during minor geomagnetic storms is strongly associated with the asymmetry features in the longitudinal distribution of solar source region for the Corotating Interaction Regions (CIR) signatures. For most of these periods of moderate geomagnetic storms, the values of MLE decreases compared to minor geomagnetic storms. This revealed that as geomagnetic stormy events build up, the level of unpredictability and sensitive dependence on initial condition (chaos) begin to decrease (Lorentz, 1963; Stogaz, 1994). The chaotic behaviour during major geomagnetic storms decreases significantly compared with moderate geomagnetic storms. The reduction in chaotic response during moderate and its further declines at major geomagnetic storms may be attributed to the disturbance in the interplanetary medium driven by sheath preceding an interplanetary coronal mass ejection (ICME) or combination of the sheath and an ICME magnetic cloud (Echer et al., 2008; Tsurutani et al., 2003; Meng et al., 2019). Notably, the dynamics of the solar wind-magnetospheric interaction are dissipative chaotic in nature (Pavlos, 2012); and, the electrodynamics of the magnetosphere due to the flux of interplanetary electric fields had a significant impact on the state of the chaotic signatures. For instance, the observation of strong chaotic behaviour during minor geomagnetic storms suggests that the dynamics was characterized by a weak magnetospheric disturbance. While the reduction in chaotic behaviour at moderate and major geomagnetic storm period reveals the dynamical features with regards to when a strong magnetospheric disturbance begins to emerge. Therefore, our observation of chaotic signatures at different categories of geomagnetic storm has potential capacity to give useful diagnostic information about monitoring space weather events. It is important to note that the features of D_{st} chaotic behaviour at different categories of geomagnetic storm has not been reported in the literature. For example, previous study of Balasis et al. (2009, 2011) investigate dynamical complexity behaviour using different entropy measures and revealed the existence of low

363 dynamical complexity in the magnetospheric dynamics and attributed it to ongoing large
364 magnetospheric disturbance (major geomagnetic storm). The work of Balasis et al. (2009, 2011)
365 where certain dynamical characteristic evolved in the D_{st} signal was revealed was limited to one
366 year data (2001). It is worthy to note that the year 2001, according to sunspot variations is a period
367 of high solar activity during solar cycle 23. It is characterized by numerous and strong solar
368 eruptions that were followed by significant magnetic storm activities. This confirms that on most
369 of the days in year 2001, the geomagnetic activity is strongly associated with major geomagnetic
370 storms. The confirmation of low dynamical complexity response in the D_{st} signal during major
371 geomagnetic storms agree with our current study. However, the idea of comparing the dynamical
372 complexity behaviour at different categories of geomagnetic storms and reveal its chaotic features
373 was not reported. This is the major reason why our present investigation is crucial to the
374 understanding of the level of chaos and dynamical complexity involved during different categories
375 of geomagnetic storms. As an extension to the single-year investigation done by Balasis et al.
376 (2009, 2011) during a major geomagnetic storm, we further investigated nine years data of D_{st}
377 that covered minor, moderate and major geomagnetic storms (see Figure 5, stem plots) and
378 unveiled their dynamical complexity behaviour. During major geomagnetic stormy periods, we
379 found that the ApEn values decrease significantly, indicating reduction in the dynamical
380 complexity behaviour. This is in agreement with the low dynamical complexity reported by Balasis
381 et al. (2009, 2011) during a major geomagnetic period. Finally, based on the method of DVV
382 analysis, we found that test of nonlinearity in the D_{st} time series during major geomagnetic storms
383 reveals the strongest nonlinearity features.

384

385

4.2 The chaotic and dynamical complexity behaviour in the VB_s as input signals.

The results of the MLE values for VB_s revealed a strong chaotic behaviour during the three categories of geomagnetic storms. Comparing these MLE values during minor to those observed during moderate and major geomagnetic storms, the result obtained did not indicate any significant difference in chaoticity (bar plots, Figure 6). Also, the ApEn values of VB_s during the periods associated with minor, moderate and major geomagnetic storms revealed high dynamical complexity behaviour with no significant difference between the three categories of geomagnetic storms investigated. These observation of high chaotic and dynamical complexity behaviour in the dynamics of VB_s may be due to interplanetary discontinuities caused by the abrupt changes in the interplanetary magnetic field direction and plasma parameters (Tsurutani et al., 2010). Also, the indication of high chaotic and dynamical complexity behaviour in VB_s signifies that the solar wind electric field is stochastic in nature. The DVV analysis for VB_s revealed nonlinearity features with no significant difference between the minor, moderate and major geomagnetic storms. It is worth mentioning that the dynamical complexity behaviour for VB_s is different from what was observed for D_{st} time series data. For instance, our results for D_{st} times series revealed that the chaotic and dynamical complexity behaviour of the magnetospheric dynamics are high during minor geomagnetic storms, reduce at moderate geomagnetic storms and further decline during major geomagnetic storms. While the VB_s signal revealed a high chaotic and dynamical complexity behaviour at all the categories of geomagnetic storm period. Therefore, these dynamical features obtained in the VB_s as input signal and the D_{st} as the output in describing the magnetosphere as a non-autonomous system further support the finding of Donner et al. (2019) that found increased or not changed in dynamical complexity behaviour for VB_s and low dynamical complexity

behaviour during storm using recurrence method. Thus, suggesting that the magnetospheric dynamics is nonlinear and the solar wind dynamics is consistently stochastic in nature.

5.0 Conclusions

This work has examined the magnetospheric chaos and dynamical complexity behaviour in the disturbance storm time (D_{st}) and solar wind electric field (VB_s) as input during different categories of geomagnetic storms. The chaotic and dynamical complexity behaviour at minor, moderate and major geomagnetic storms for solar wind electric field (VB_s) as input and D_{st} as output of the magnetospheric system were analyzed for the period of 9 years using nonlinear dynamics tools. Our analysis has shown a noticeable trend of these nonlinear parameters (MLE and ApEn) and the categories of geomagnetic storm (minor, moderate and major). The MLE and ApEn values of the D_{st} have indicated that the chaotic and dynamical complexity behaviour are high during minor geomagnetic storms, low during moderate geomagnetic storms and further reduced during major geomagnetic storms. The values of MLE and ApEn obtained from VB_s indicate that chaotic and dynamical complexity are high with no significant difference during the periods of minor, moderate and major geomagnetic storms. Finally, the test for nonlinearity in the D_{st} time series during major geomagnetic storms reveals the strongest nonlinearity features. Based on these findings, the dynamical features obtained in the VB_s as input and D_{st} as output of the magnetospheric system suggest that the magnetospheric dynamics is nonlinear and the solar wind dynamics is consistently stochastic in nature.

7.0 Acknowledgement

The authors would like to acknowledge the World Data Centre for Geomagnetism, Kyoto, and the National Aeronautics and Space Administration, Space Physics Facility (NASA) for making the Dst data and solar wind plasma data available for research purpose. Also, the efforts of anonymous reviewers in ensuring that the quality of the work is enhanced are highly appreciated.

Declaration of Interest statement

The authors declare that there is no conflicts of interest.

References

Akasofu, S.I., (1964), The development of the auroral substorm. Planet. Space Sci., 12, 273-282, doi:10.1016/0032-0633(64)90151-5.

Baker, D.N., Klimas, A.J., (1990). The evolution of weak to strong geomagnetic activity: An interpretation in terms of deterministic chaos. J. GeoPhys. Res. Letts. Vol. 17, No. 1, PP. 41-44.

Balasis, G., Daglis, I.A., Anastasiadia, A., Eftaxias, K., (2011). Detection of dynamical complexity changes in Dst time series using entropy concepts and rescaled range analysis. W.Liu, M. Fujimoto (eds.), The Dynamics Magnetosphere, IAGA Special Sopron Book Series 3, doi: 10.1007/978-94-007-0501-2_12, Springer Science+Business Media B.V. 2011.

Balasis, G., I.A. Daglis, C. Papadimitriou, M. Kalimeri, A. Anastasiadis, K. Eftaxias (2009). Investigating dynamical complexity in the magnetosphere using various entropy measures, J.Geophys.Res., 114, A0006, doi: 10.1029/2008JA 014035.

Balasis, G., I.A. Daglis, P. Kapiris, M.Mandea, D. Vassilliadis, K. Eftaxias (2006). From pre-storm activity to magnetic storms: a transition described in terms of fractal dynamics, Ann.Geophys., 24, 3557-3567, www.ann-geophys.net/24/3557/2006.

Balikhin, M.A., Boynton, R.J., Billings, S.A., Gedalin, M., Ganushkina, N., Coca, D., (2010). Data based quest for solar wind-magnetosphere coupling function, Geophys.Res.Lett, 37, L24107, doi: 10.1029/2010GL045733.

Burton, R.K., McPherron, R.L., Russell, C.T., (1975). An empirical relationship between interplanetary conditions and Dst. Journal of Geophysical Research, Vol.80, No.31.

Consolini, G., (2018), Emergence of dynamical complexity in the Earth's magnetosphere, Machine learning techniques for space weather, PP. 177-202, doi: 10.1016/B978-0-12-811788-0.00007-X

Cowley, S.W.H., (1995). The earth's magnetosphere: A brief beginner's guide, EOS Trans.Am.GeoPhys.Union, 76, 525.

Dessler, A.J., Parker, E.N., (1959). Hydromagnetic theory of magnetic storm. J. GeoPhys. Res, 64, PP 2239-2259.

Devi, S.P., Singh, S.B., Sharma, A.S., (2013). Deterministic dynamics of the magnetosphere: results of the 0-1 test. Nonlin. Processes Geophys., 20, 11-18, 2013, www.nonlin-processes-geophys.net/20/11/2013, doi: 10. 5194/npg-20-11-2013.

Donner, R.V., Balasis, G., Stolbova,V., Georgiou, M., Weiderman, M., Kurths, J. (2019). Recurrence-based quantification of dynamical complexity in the earth's magnetosphere at

geospace storm time scales. Journal of Geophysical Research: Space Physics, 124, 90-108, doi: 10.1029/2018JA025318.

Dungey, J.W., (1961). Interplanetary magnetic field and auroral zones. Phys.Rev.Lett., 6, 47, doi: 10.1103/PhysRevLett.6.47

Echer, E., Gonzalez, D., Alves, M.V., (2006). On the geomagnetic effects of solar wind interplanetary magnetic structures. Space Weather, Vol.4, S06001, doi:10.1029/2005SW000200.

Echer, E., Gonzalez, W.D., Tsurutani, B.T., Gonzalez, A. L. C., (2008), Interplanetary conditions causing intense geomagnetic storms ($D_{st} \leq -100nT$) during solar cycle 23 (1996–2006), J. Geophys. Res., 113, A05221, doi:10.1029/2007JA012744.

Feldstein, Y.I., Levitin, A.E., Kozyra, J.U., Tsurutani, B.T., Prigancova, L., Alperovich, L., Gonzalez, W.D., Mall, U., Alexeev, I.I., Gromava, L.I., Dremukhina, L.A., (2005). Self-consistent modelling of the large-scale distortions in the geomagnetic field during the 24-27 September 1998 major geomagnetic storm. JGR, 110, A11214, doi: 10.1029/2004JA010584.

Feldstein, Y.I., Popov, V.A., Cumnock, J.A., Prigancova, A., Blomberg, L.G., Kozyra, J.U., Tsurutani, B.T., Gromova, L.I., Levitin, A.E., (2006). Auroral electrojets and boundaries of plasma domains in the magnetosphere during magnetically disturbed intervals. Ann. Geophys., 24, 2243-2276, www.ann-geophys.net/24/2243/2006/

Fraser, A.M., (1986). Using mutual information to estimate metric entropy, dimension and entropies in chaotic system, Springer-Verlag, 1986, PP: 82-91.

Fraser, A.M., Swinney, H.L., (1986). Independent coordinates for strange attractors from mutual information, Phys.Rev.A 33, 1134-1140.

Gautama, T., Mandic, D.P., Hulle, M.M.V., (2004). The delay vector variance method for detecting determinism and nonlinearity in time series. Physica D, 190, 167-176, doi: 10.1016/j.physd.2003.11.001.

Gonzalez, W.D., Joselyn, J.A., Kamide, Y., Kroehl, H.W., Rostoker, G., Tsurutani, B.T., Vasyliunas, V.M., (1994). What is a geomagnetic storm? J. Geophys. Res.: Space Physics, Vol. 99, issue A4, pg. 5771-5792, doi: 10.1029/93JA02867.

Gonzalez, W.D., Tsurutani, B.T., (1987). Criteria of interplanetary parameters causing intense magnetic storm ($Dst < -100nT$). Planetary and Space Science, https://ntrs.nasa.gov/search.jsp?R=198800068.

Gonzalez, W.D., Tsurutani, B.T., Gonalez, A.L.C., Smith, E.J., Tang, F., Akasofu, S.I., (1989). JGR, 94, A7, 8835-8851, doi: 10.1029/JA094iA07p08835.

Hajra, R., Echer, E., Tsurutani, B.T., Gonazalez, W.D., (2013). Solar cycle dependence of High-intensity Long-duration Continuous AE activity (HILDCAA) events, relativistic electron predictors? (2013), JGR, Space Physics, 118, 5626-5638, doi: 10.1002/jgra.50530.

Hajra, R., Tsurutani, B.T., (2018), Interplanetary shocks inducing magnetospheric supersubstorms (SML<-2500nT): unusual auroral morphologies and energy flow. The AstroPhysical Journal, 858:123(6pp), doi:10.3847/1538-4357/aabaed.

509 Horne, R.H., Glauert, S.A., Meredith, N.P., Boscher, D., Maget, V., Heynderickx, D., and Pitcford,
510 D. (2013). Space weather impacts on satellites and forecasting the Earths electron radiation
511 belts with SPACECAST. Space weather, **11,** 169 - 186

512 Imtiaz, A., (2010). Detection of nonlinearity and stochastic nature in time series by delay vector
513 variance method, International journal of Engineering & Technology, Vol. 10, No. 02.

514 Jaksic, V., Mandic, D.P., Ryan, K., Basu, B., Pakrashi V., (2016). A Comprehensive Study of the
515 Delay Vector Variance Method for Quantification of Nonlinearity in dynamical Systems.
516 *R.Soc.OpenSci.*, 2016: 3:150493, http://dx.doi.org/10.1098/rsos.150493.

517 Johnson, J.R., Wing, S., (2005), A solar cycle dependence of nonlinearity in magnetospheric
518 activity. J. Geophys. Res., 110, A04211, doi: 10.1029/2004JA010638.

519 Kannathal, N., M.L. Choo, U. R. Acharya, P. K. Sadasivan (2005). Entropies for detecting of
520 epilepsy in EEG, Computer Methods and Programs in Biomedicine (2005) 80, 187-194,
521 www.intl.elsevierhealth.com/journals/cmpb.

522 Kennel, M.B., R. Brown, H.D.I. Abarbanel (1992). Determining embedding dimension for phase-
523 space reconstruction using a geometrical construction, PHYSICAL REVIEW A, Volume 45,
524 Number 6.

525 Klimas, A.J., Vassilliasdis, D., Baker. D.N., Roberts, D.A., (1996). The organized nonlinear
526 dynamics of the magnetosphere. J. GeoPhys. Res. Vol.101, No. A6, PP 13089-13113.

527 Kozyra, J.U., Crowley, G., Emery, B.A., Fang, X., Maris, G., Mlynczak, M.G., Niciejewski, R.J.,
528 Palo, S.E., Paxton, L.J., Randall, C.E., Rong, P.P., Russell, J.M., Skinner, W., Solomon, S.C.,
529 Talaat, E.R., Wu, Q., Yee, J.H., (2006), Response of the Upper/Middle Atmosphere to Coronal

530 Holes and Powerful High-Speed Solar Wind Streams in 2003, Geophysical Monograph Series
531 167, 10.1029/167GM24.

532 Kugiumtzis, D., (1999). Test your surrogate before you test your nonlinearity, Phys. Rev. E, 60,
533 2808-2816.

534 Liou, K., Newell, P.T., Zhang, Y.-L., Paxton, L.J., (2013), Statistical comparison of isolated and
535 non-isolated auroral substorms. J. Geophys. Res. Space Physics, 118, 2466-2477, doi:
536 10.1002/jgra.50218.

537 Lorenz, E.N., (1963). Determining nonperiodic flow. J. Atmos.Sci.,20,130.

538 Love, J.J., Gannon, J.L. (2009). Revised Dst and the epicycles of magnetic disturbance: 1958-2007.
539 Ann.GeoPhys., 27, 3101-3131.

540 Mandic, D.P., Chen, M., Gautama, T., Van Hull, M.M., Constantinides, A., (2007). On the
541 Characterization of the Deterministic/Stochastic and Linear/Nonlinear Nature of Time Series.
542 *Proc.R.Soc*, 2008: A464, 1141-1160, doi: 10.1098/rspa. 2007.0154.

543 Mane, R., (1981). On the dimension of the compact invariant sets of certain nonlinear maps, D.Rand
544 and L.S.Young, eds, 1981.

545 Mckinley, R.A., Mclntire, L.K., Schmidt, R., Repperger, D.W., Caldwell, J.A., (2011). Evaluation
546 of Eye Metrics as a Detector of Fatigue. Human factor, 53 (4): 403-414, doi:
547 10.1177/0018720811411297.

548 Mendes, O., Domingues, M.O., Echer, E., Hajra, R., Menconi, V. E., (2017). Characterization of
549 high-intensity, long-duration continuous auroral activity (HILDCAA) events using recurrence

550 quantification analysis. Nonlin. Processes Geophys., 24, 407-417, doi: 10.5194/npg-24-407-
551 2017.

552 Mendes, O., Dominques, M.O., Echer, E., Hajra, R., Menconi, V.E., (2017), Characterization of
553 high-intnesity, long-duration continuous auroral activitity (HILDCAA) events using
554 recurrence quantification analysis. Nonlin. Processes Geophys.,24,407-417, doi:10.5194/npg-
555 24-407-2017.

556 Meng, C. I., Tsurutani, B., Kawasaki, K., Akasofu, S. I., (1973), Cross-correlation analysis of the
557 AE index and the interplanetary magnetic field Bz component. Journal of Geophysical
558 Research, Vol. 78., No 4., doi: 10.1029/JA078i004p00617.

559 Meng, X., Tsurutani, B. T., Mannucci, A. J. (2019). The solar and interplanetary causes of
560 superstorms (minimum Dst ≤ −250 nT) during the space age. Journal of Geophysical Research:
561 Space Physics, 124, 3926–3948. https://doi.org/10.1029/2018JA026425.

562 Millan, H., Gharbarian-Alavijeh, B., Garcia-Fornaris, I., (2010). Nonlinear dynamics of mean daily
563 temperature and dewpoint time series at Babolsar, Iran, 1961-2005. Elsevier, Atmospheric
564 Research 98 (2010) 89-101, doi: 10.1016/j.atmosres.2010.06.001.

565 Moore, C., Marchant, T., (2017). The approximate entropy concept extended to three dimensions
566 for calibrated, single parameter structural complexity interrogation of volumetric images.
567 Physics in Medicine & Biology, 62(15).

568 Oludehinwa, I.A., Olusola, O.I., Bolaji, O.S., Odeyemi, O.O., (2018). Investigation of nonlinearity
569 effect during storm time disturbance, Adv. Space. Res, 62 (2018) 440-456, doi:
570 10.1016/j.asr.2018.04.032.

571 Omkar, P.T., Verma, P.L., (2013). Solar features and solar wind plasma parameters with
572 geomagnetic storms during the period of 2002-2006. Indian Journal of Applied Research,
573 Vol.3, Issue.5, ISSN-2249-555X.

574 Pavlos, G.P., (1994). The magnetospheric chaos: a new point of view of the magnetospheric
575 dynamics. Historical evolution of magnetospheric chaos hypothesis the past two decades.
576 Conference Proceeding of the 2nd Panhellenic Symposium held in Democritus University of
577 Thrace, Greece, 26-29, April, edited 1994.

578 Pavlos, G.P., (2012). Magnetospheric dynamics and Chaos theory

579 Pavlos, G.P., Athanasiu, M.A., Diamantidis, D., Rigas, A.G., Sarri, E.T., (1999). Comments and
580 new results about the magnetospheric chaos hypothesis. Nonlinear Processes in Geophysics
581 (1999) 6: 99-127.

582 Pavlos, G.P., Rigas, A.G., Dialetis, D., Sarris, E.T., Karakatsanis, L.P., Tsonis, A.A., (1992).
583 Evidence of chaotic dynamics in the outer solar plasma and the earth magnetosphere. Chaotic
584 dynamics: Theory and Practice, Edited by T. Bountis, Plenum Press, New York, Page. 327-
585 339, doi:10.1007/978-1-4615-3464-8_30.

586 Pincus, S.M., (1991). Approximate entropy as a measure of system complexity, Proc.Natl.Acad.Sci.
587 USA, Vol.88, PP. 2297-2301.

588 Pincus, S.M., Goldberger, A.L., (1994). Physiological time series analysis: what does regularity
589 quantify, The American Journal of Physiology, 266 (4): 1643-1656.

590 Pincus, S.M., Kalman, E.K., (2004). Irregularity, volatility, risk, and financial market time series,
591 Proceedings of the National Academy of Sciences, 101 (38): 13709-13714, doi:
592 10.1073/pnas.0405168101.

593 Price, C.P., Prichard, D., Bischoff, J.E., (1994). Nonlinear input/output analysis of the auroral
594 electrojet index. Journal of Geophysical Research, Vol.99, No: A7, PP: 227-238.

595 Price,C.P., Prichard, D., (1993). The Non-linear response of the magnetosphere: 30 October, 1978.
596 Geophysical Research Letters, Vol.20.

597 Richardson, I.G., Cane, H.V., (2011), Geoeffectiveness (D_{st} and K_p) of interplanetary coronal
598 mass ejections during 1995-2009 and implication for storm forecasting, Space Weather, 9,
599 S07005, doi:10.1029/2011SW000670.

600 Russell, C.T., (2001). Solar wind and Interplanetary Magnetic Field: A Tutorial. Space Weather,
601 Geophysical Monograph 125, Page: 73-89.

602 Russell, C.T., McPherron, R.L., Burton, R.K. (1974). On the cause of geomagnetic storms,
603 J.GeoPhys.Res., 79, 1105-1109.

604 Shujuan G., Weidong, Z., (2010). Nonlinear feature comparison of EEG using correlation
605 dimension and approximate entropy, 3rd international conference on biomedical engineering
606 and informatics.

607 Strogatz, S.H., (1994), Nonlinear dynamics and chaos with Application to physics, Biology,
608 chemistry and Engineering, New York, John Wiley & Sons.

609 Sugiura, M. (1964). Hourly Values of equatorial Dst for the IGY, Ann.Int. GeoPhys. Year, 35, 9-
610 45.

611 Takens, F., (1981). Detecting Strange Attractors in Turbulence in Dynamical Systems, D.*Rand &*
612 *L.Young Eds*, 1981: 898, 366-381.

613 Theiler, J., Eubank, S., Longtin, A., Galdrikian, B., Farmer, J.D., (1992), Testing for nonlinearity
614 in time series: The method of surrogate data, Physica D, 58, 77.

615 Tsurutani, B. T., Meng, C. I., (1972), Interplanetary magnetic field variations and substorm activity.
616 Journal of Geophysical Research, Vol. 77., No 16., doi: 10.1029/JA077i016p029.

617 Tsurutani, B.T., Gonazalez, W.D., (1987), The cause of High-intensity Long duration Continuous
618 AE activity (HILDCAAs): Interplanetary Alfven trains. Planet. Space Sci., 35, 4, 405-412, doi:
619 10.1016/0032-0633(87)90097-3.

620 Tsurutani, B.T., Gonzalez, A.L.C., Tang, F., Arballo, J.K., Okada, M., (1995), Interplanetary origin
621 of geomagnetic activity in the declining phase of the solar cycle. JGR, 100, A11, 717-733,
622 95JA01476.

623 Tsurutani, B.T., Gonzalez, W. D., Tang, F., Akasofu, S.I., Smith, E.J., (1988), Origin of
624 Interplanetary Southward Magnetic Fields Responsible for Major Magnetic Storms Near Solar
625 Maximum (1978-1979), Journal of Geophysical Research, Vol. 93, No. A8, Pages 8519-8531,
626 Paper number 7A9404, 0148-0227/88/007 A-9404$05.00.

627 Tsurutani, B.T., Gonzalez, W.D., Lakhina, G.S. Alex, S., (2003). The extreme magnetic storm of
628 1-2 September 1859, J. Geophys. Res. 108(A7), doi: 10.1029/2002JA009504.

629 Tsurutani, B.T., Hajra, R., (2021). The interplanetary and magnetospheric causes of
630 geomagnetically induced currents (GICs) >10A in the Mantsala finland Pipeline: 1999
631 through 2019. J. Space Weather Space Clim, 11, 23, doi: 10.1051/swsc/2021001.

632 Tsurutani, B.T., Lakhina, G.S., Hajra, R., (2020), The physics of space weather/solar-terrestrial
633 physics (STP): what we know now and what the current and future challenges are, Nonlin.
634 Processes Geophys., 27, 75–119, doi:10.5194/npg-27-75-2020.

635 Tsurutani, B.T., Lakhina, G.S., Verkhoglyadova, O.P., Gonzalez, W.D., Echer, E., Guarnieri, F.L.,
636 (2010). A review of interplanertary discontinuities and their geomagnetic effects. Journal of
637 Atmospheric and Solar-Terrestrial Physics, doi: 10.1016/j.jastp.2010.04.001.

638 Tsurutani, B.T., Sugiura, M., Iyemori, T., Goldstein, B.E., Gonazalez, W.D., Akasofu, S.I., Smith,
639 E.J., (1990). The nonlinear response of AE to the IMF Bs driver: A spectral break at 5 hours.
640 Geophysical Research Letters, Vol.17, No.3., Pages: 279-283.

641 Tsutomu, N., (2002). Geomagnetic storms. Journal of communications Research Laboratory, Vol.
642 49, No.3.

643 Turner, N.E., Mitchell, E.J., Knipp, D.J., Emery, B.A., (2006), Energetics of magnetic storms
644 driven by corotating interaction regions: a study of geoeffectiveness, Geophysical Monograph
645 Series 167, 10.1029/167GM11.

646 Unikrishnan, K., (2008). Comparison of chaotic aspect of magnetosphere under various physical
647 conditions using AE index time series. Ann. Geophys., 26, 941-953, www.ann-
648 geophys.net/26/941/2008.

649 Unikrishnan, K., Ravindran, S., (2010). A study on chaotic behaviour of equatorial/low latitude
650 ionosphere over indian sub-continent, using GPS-TEC time series, J. Atmos. Sol. Ter. Phys.,
651 72, 1080-1089.

652 Valdivia, J.A., Rogan, J., Munoz, V., Gomberoff, L., Klimas, A., Vassilliasdis, D., Uritsky, V.,
653 Sharma, S., Toledo, B., Wastaviono, L. (2005). The magnetosphere as a complex system. Adv.
654 Space. Res, 35, 961-971.

655 Valdivia, J.A., Sharma, A.S., Papadopoulos, K., (1996). Prediction of magnetic storms by nonlinear
656 models. Geophysical Research Letters, 23(21), 2899-2902, doi: 10.1029/96GL02828.

657 Vassiliadis, D., (2006). Systems theory for geospace plasma dynamics, Rev.Geophys., 44, RG2002,
658 doi: 10.1029/2004RG000161.

659 Vassiliadis, D., Klimas, A.J., Valdivia, J.A., Baker, D.N., (1999). The geomagnetic response as a
660 function of storm phase and amplitude and solar wind electric field. Journal of Geophysical
661 Research, 104(A11), 24957-24976, doi: 10.1029/1999JA900185.

662 Vassilliadis, D., Sharma, A.S., Papadopoulos, K., (1991). Lyapunov exponent of magnetospheric
663 activity from AL time series. J. GeoPhys. Letts, Vol. 18, No.8, PP. 1643-1646.

664 Vassilliadis, D.V., Sharma, A.S., Eastman, T.E., Papadopoulou, K., (1990). Low-dimensional
665 chaos in magnetospheric activity from AE time series. J. GeoPhys.Res.Lett, 17, 1841-1844.

666 Wallot, S., Monster, D., (2018). Calculation of Average Mutual Information (AMI) and False
667 Nearest Neigbhours (FNN) for the estimation of embedding parameters of multidimensional
668 time series in MATLAB. Front. Physchol. 9:1679, doi: 10.3389/fpsyg.2018.01679.

669 Watari, S., (2017). Geomagnetic storms of cycle 24 and their solar sources, Earth, Planets and
670 Space, PP: 69:70, doi: 10.1186/s40623-017-0653-z.

671 Wolf, A., Swift, J. B., Swinney, H. L., and Vastano, J. A. (1985). Determining Lyapunov exponents
672 from a time series, *Physica D, 16*, 285–317, doi:10.1016/0167-2789(85)90011-9.

673 Zhang, J., Dere, K.P., Howard, R.A., Bothmer, V., (2002), Identification of solar sources of major
674 geomagnetic storms between 1996 and 2000. Astrophysical Journal, 582:520-53.

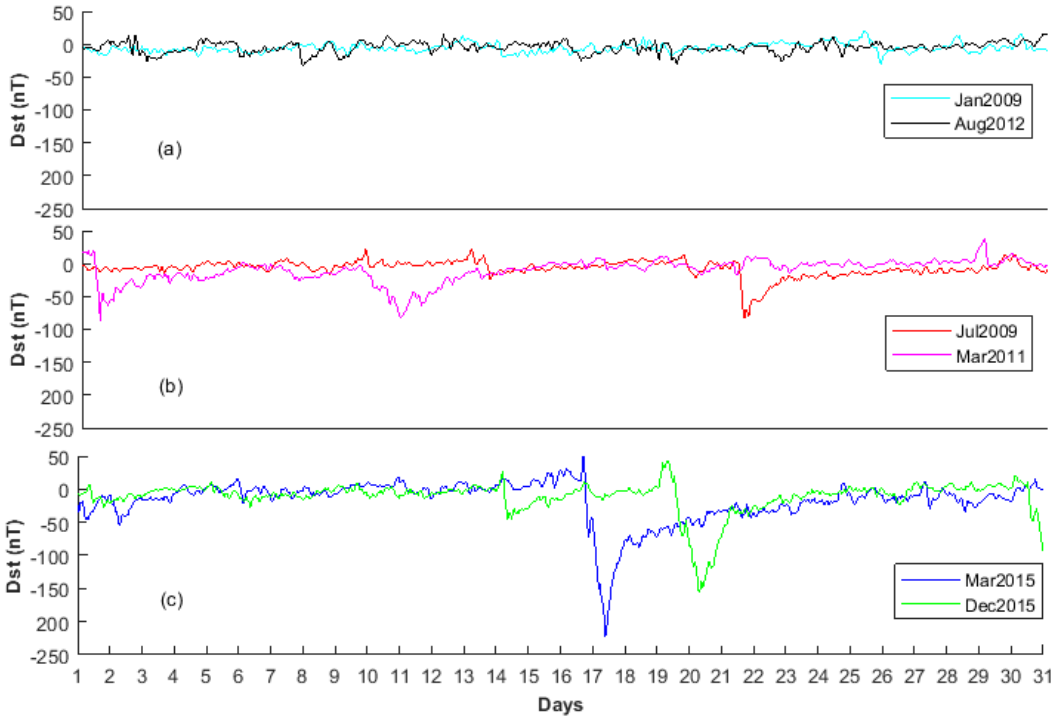

Figure 1: Samples of D_{st} signals classified as (a) Minor, (b) Moderate and (c) Major geomagnetic storm

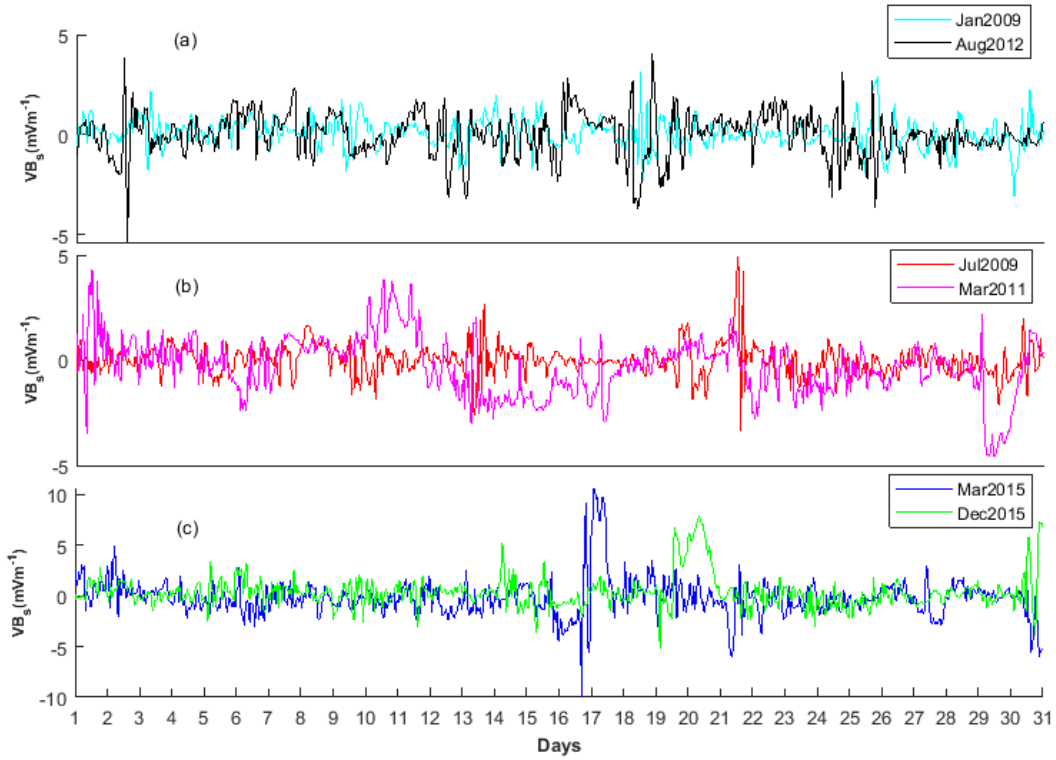

Figure 2: Samples of solar wind electric fields (VB_s) during (a) Minor, (b) Moderate and (c) Major geomagnetic storm.

681

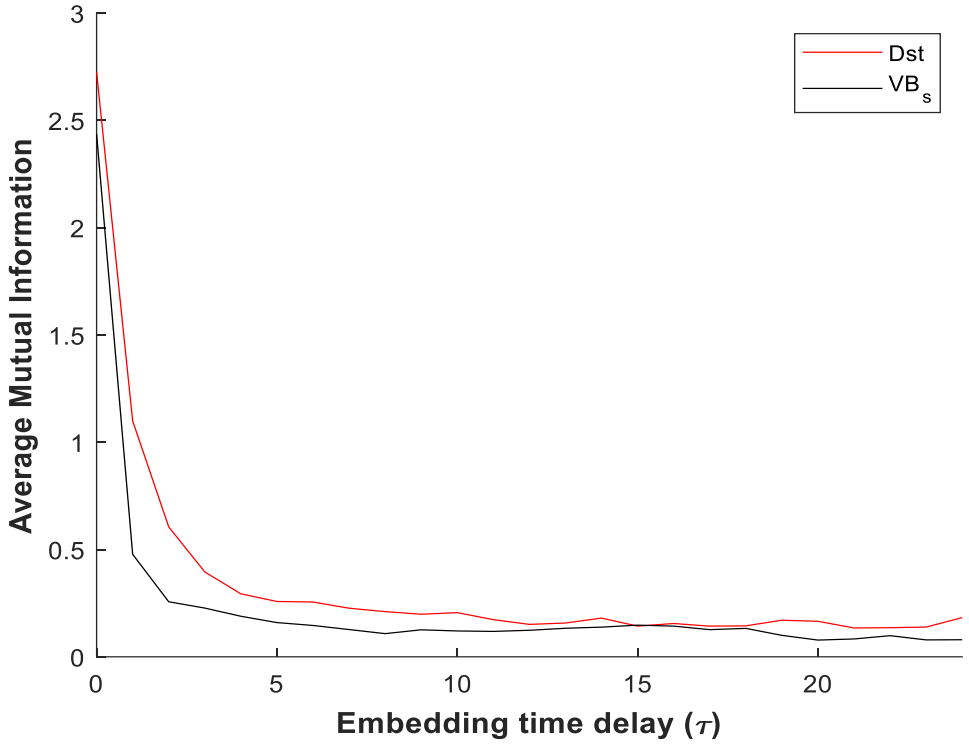

682

683 Figure 3: The plot Average Mutual Information against embedding time delay (τ)

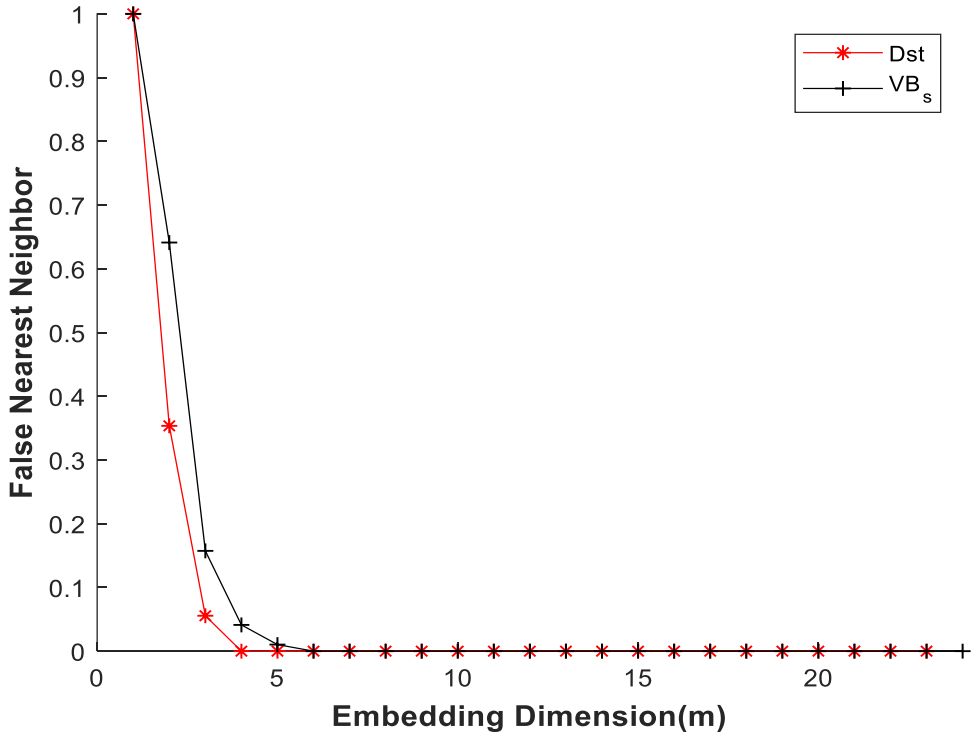

684

685 Figure 4: The plot of Percentage of False Nearest Neighbors against embedding dimension (m)

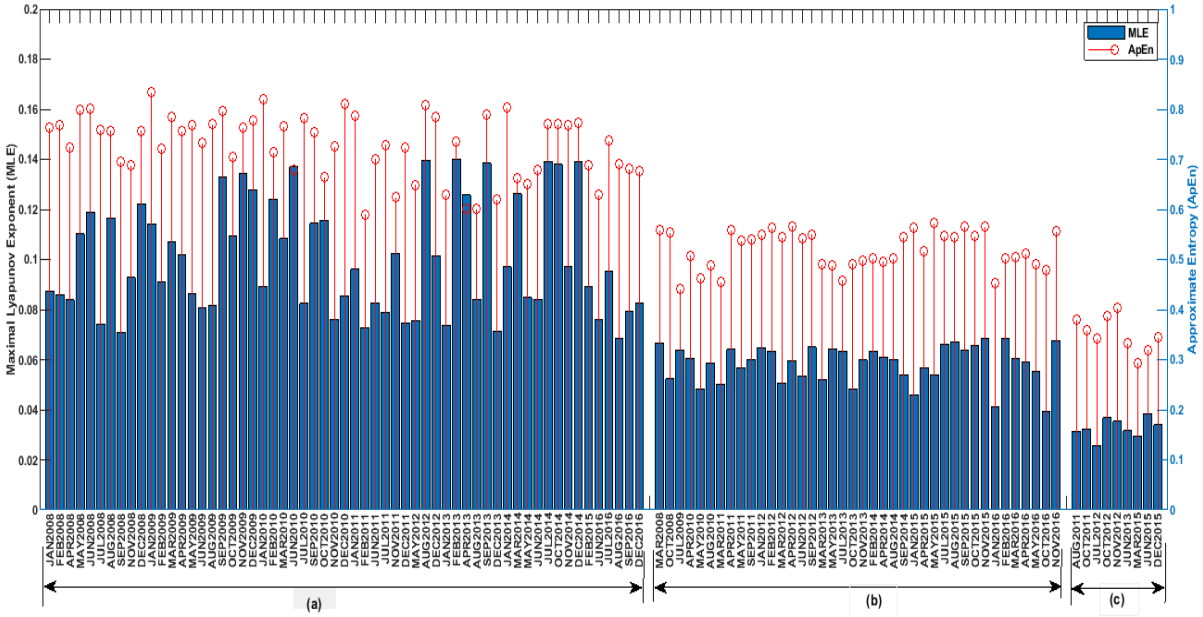

Figure 5: The MLE (bar plot) and ApEn (stem plot) of D_{st} at: (a) Minor, (b) Moderate and (c) Major geomagnetic storm.

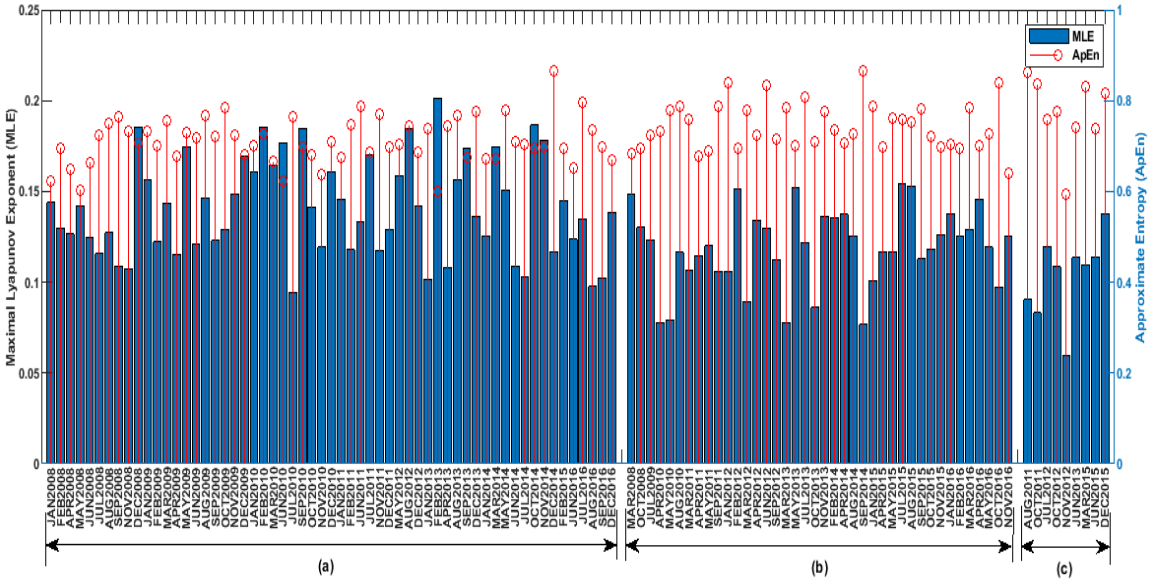

Figure 6: The MLE (bar plot) and ApEn (stem plot) of solar wind electric field (VB_s) during: (a) Minor, (b) Moderate and (c) Major geomagnetic storm.

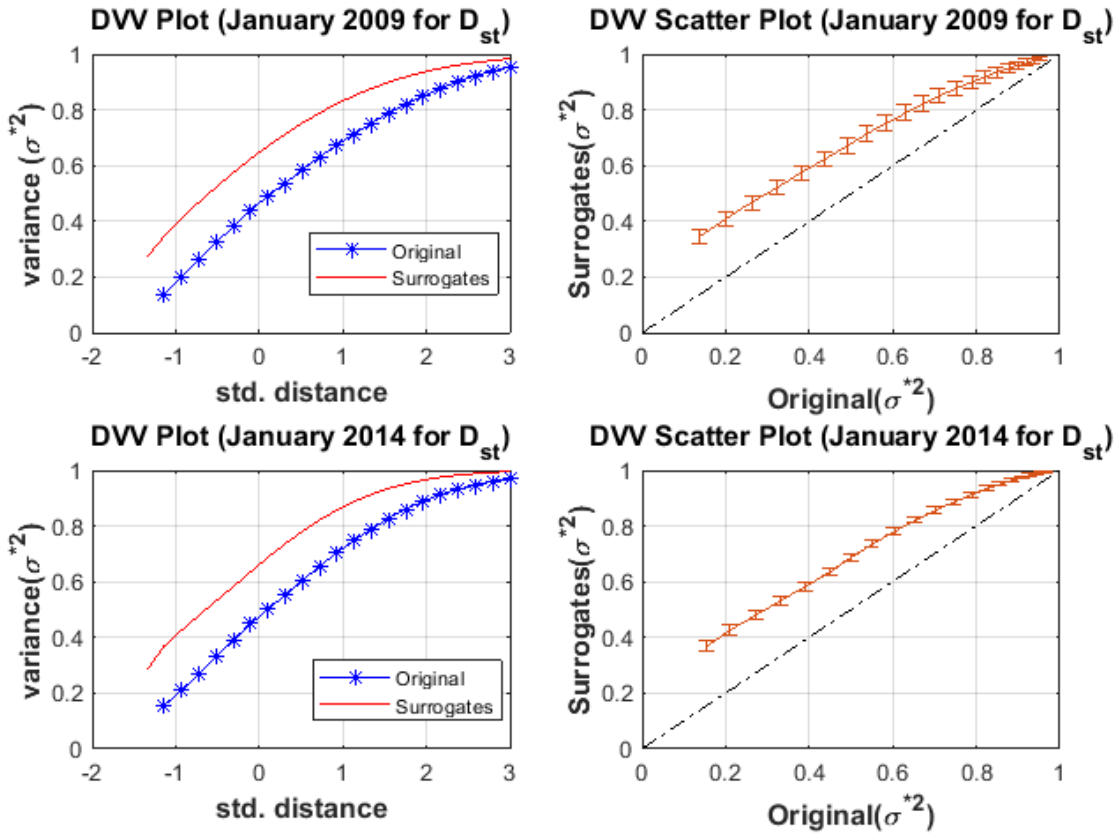

712

713 Figure 7: The DVV plot and Scatter plot for D_{st} during minor geomagnetic storm for January
714 2009 and January 2014.

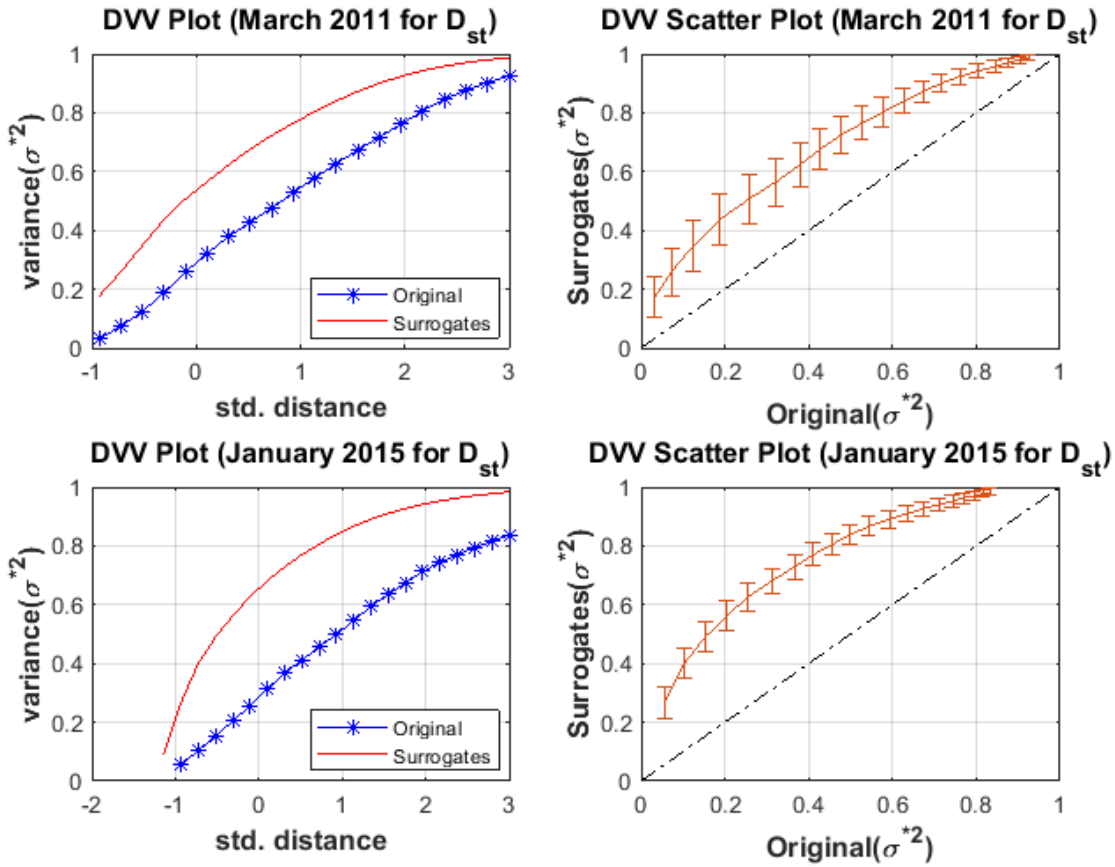

715

716

717 Figure 8: The DVV plot and Scatter plot for D_{st} during moderate geomagnetic storm for March
718 2011 and January 2015.

719

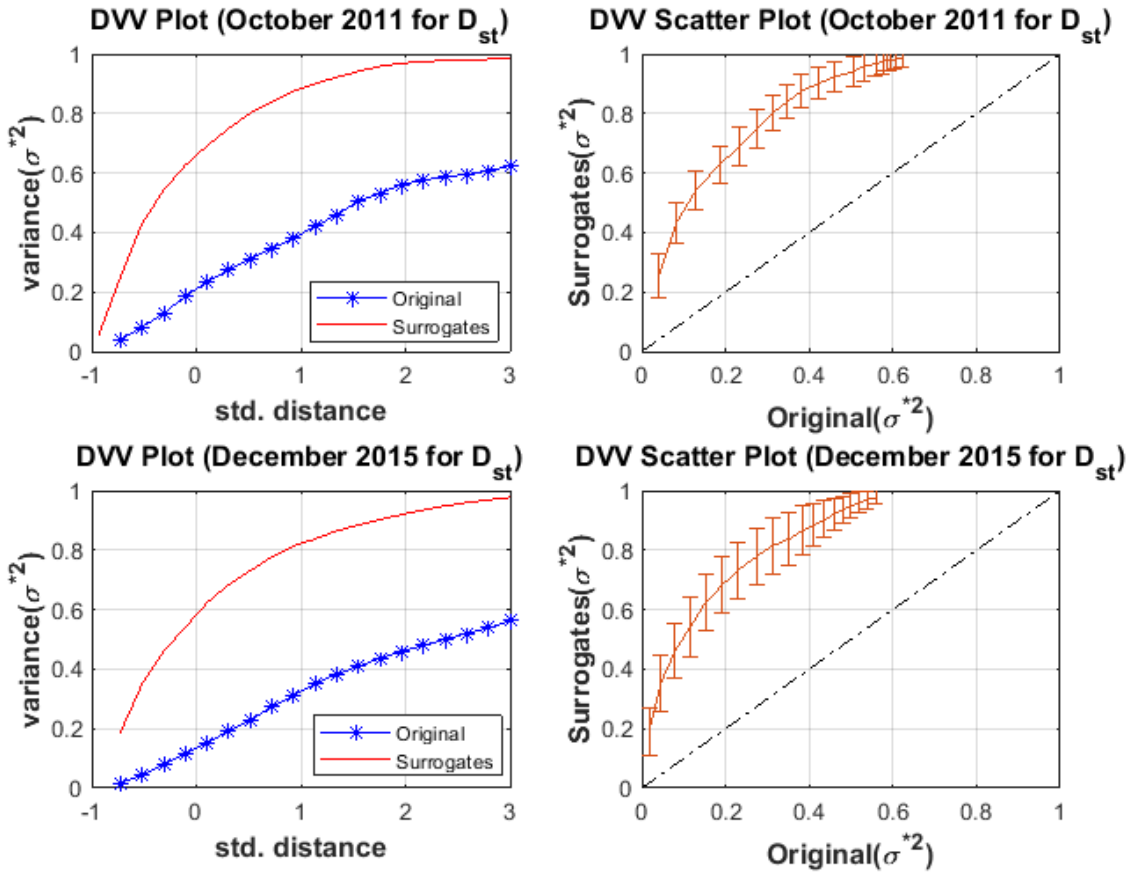

720

721 Figure 9: The DVV plot and Scatter plot for D_{st} during major geomagnetic storm for October
722 2011 and December 2015.

723

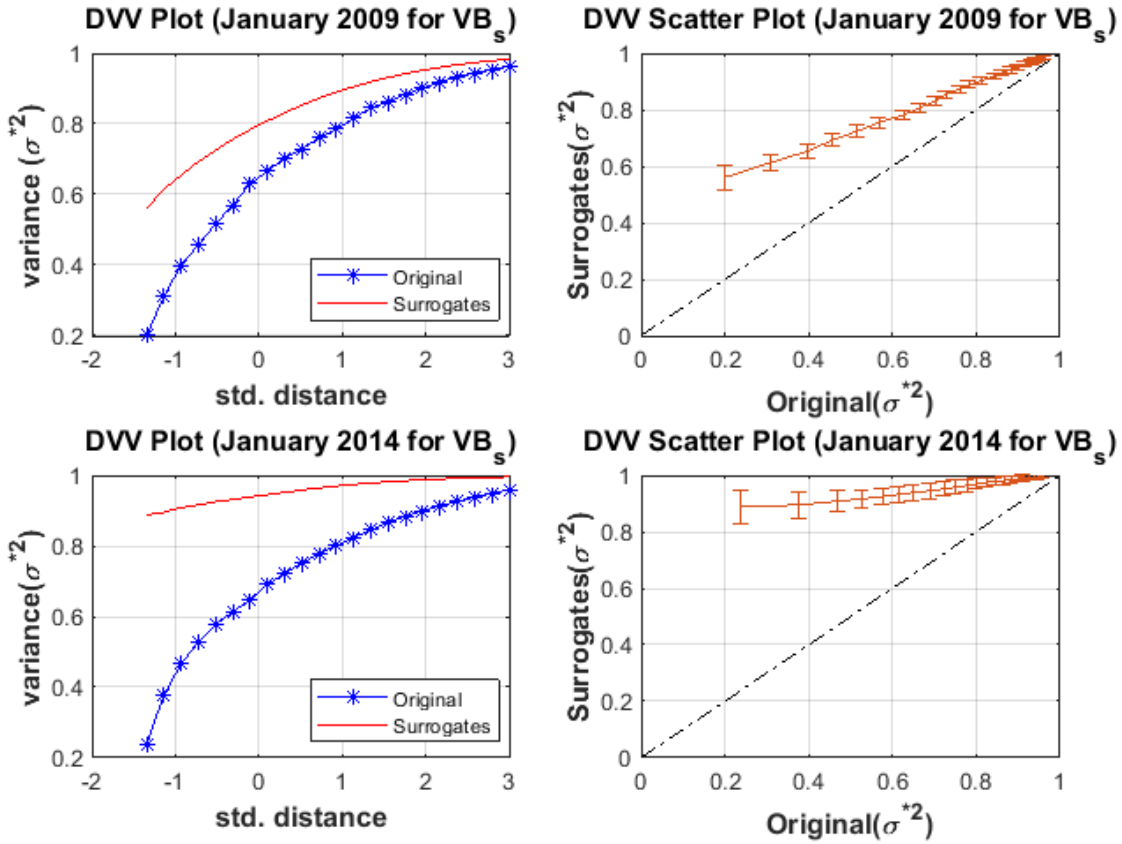

Figure 10: The DVV plot and Scatter plot for VB_s during minor geomagnetic storm for January 2009 and January 2014.

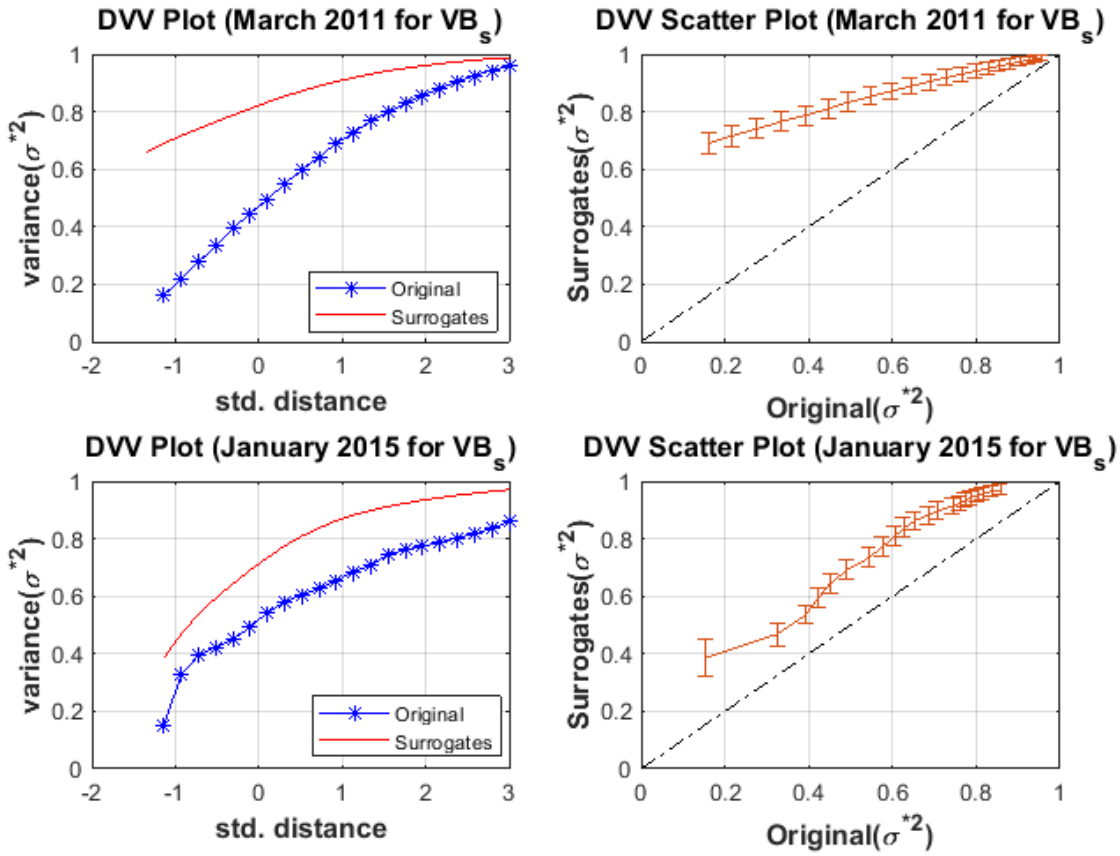

729

730 Figure 11: The DVV plot and Scatter plot for VB_s during moderate geomagnetic storm for March
731 2011 and January 2015.

732

733

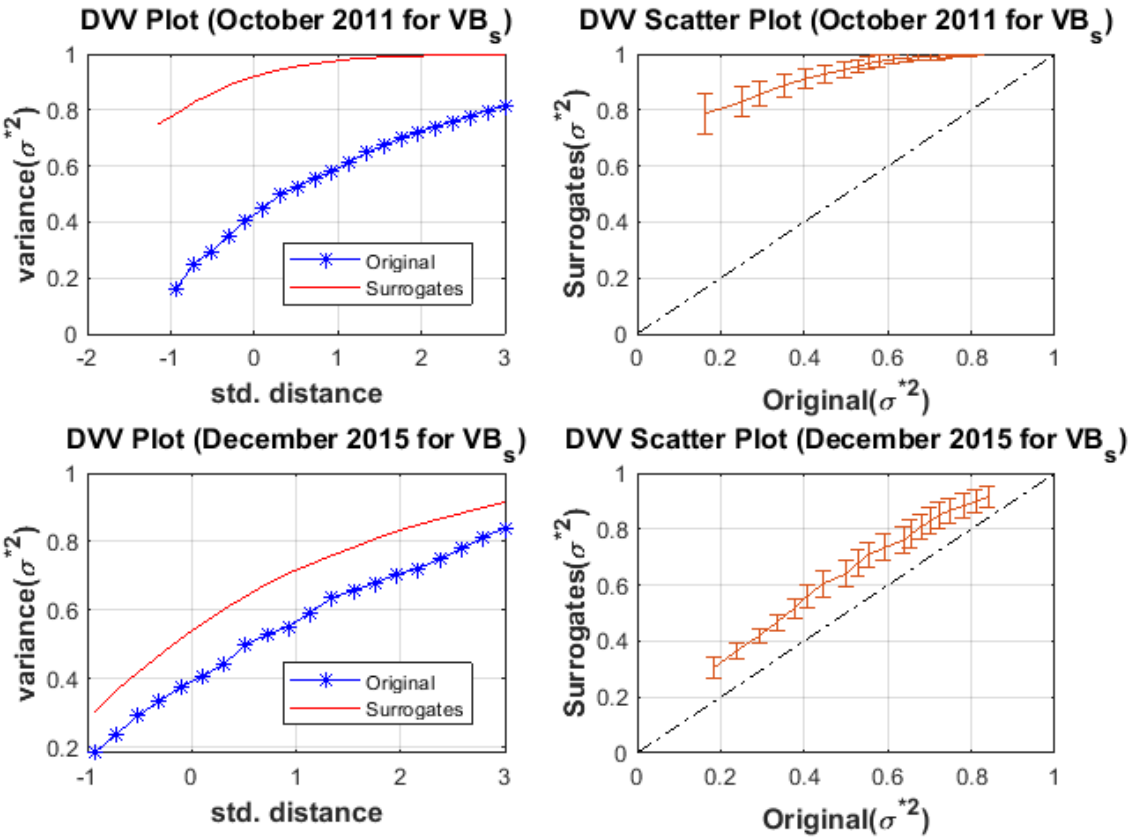

734

735 Figure 12: The DVV plot and Scatter plot for VB_s during major geomagnetic storm for October
736 2011 and December 2015.

737

738

739